Implemented Optical Perfect Shuffle with A Planarized Architecture

Jian Liu, Degui Sun, Chunhe Zhao, and Ray T. Chen

Microelectronics Research Center
Department of Electrical and Computer Engineering
University of Texas at Austin
Austin, Texas 78758

ABSTRACT

In this paper, a substrate-guided-wave-based Perfect Shuffle (PS) having an 8-to-8 interconnection is demonstrated at 632.8 nm wavelength. Sixteen waveguide holograms are fabricated on a planar waveguiding plate with the full functionality of the PS. The diffraction efficiencies of the waveguide holograms are all within 80% ± 5%. The planar architecture combined with the surface-normal configuration of the demonstrated PS makes the integration with vertical cavity surface emitting lasers (VCSELs) and other surface mountable processing elements highly feasible.

Key words: optical perfect shuffle, volume hologram, optical interconnects, photopolymer films, parallel processing.

1. Introduction

In parallel computing architecture, the perfect shuffle (PS) is proven to be an efficient interconnection method for parallel processing algorithms, such as the fast-Fourier transform (FFT), polynomial evaluation, sorting, and matrix transposition.[1] For high-speed (> 1 GHz) parallel processing, the performance of the existing communication links among processing elements (PEs) based on microelectronic integrated circuits is limited by electromagnetic interference, parasitic capacitance, and inductance coupling. To overcome the bottlenecks of electrical interconnects, optical interconnection has been widely agreed to be one of the most important alternatives.[2,3]

Many investigators have been working on optical implementation of the perfect shuffle, and several approaches have been proposed and then demonstrated.[4-9] Lohmann and his colleague[4,5] performed this concept with a combination of lenses and prisms. Using microlens arrays, the PS is demonstrated by Sawchuk and Glaser.[6] Recently, holographic optical elements (HOEs) are employed to implement one-dimensional (1-D) and two-dimensional (2-D) PSs.[7-9] All these implementations are limited to free space optical interconnects, which are vulnerable to mechanical and environmental perturbations. Furthermore, extra components like lenses and/or prisms are always needed to route optical signals. These

SPIE Vol. 3159 • 0277-786X/97/$10.00

architectures are not easily compatible with the surface mount technology (SMT) for which the planarization is required.

Substrate guided wave optical interconnects, using HOEs combined with total internal reflection (TIR) in dielectric or semiconductor substrates, have been demonstrated as efficient approaches for intra- and inter-module interconnections, optical clock distributions, and optical backplane buses.[10] This approach provides an planarized architecture with surface normal configuration, which makes easy the integration with VCSEL arrays, and other surface-mountable processing elements. In this paper, we present the PS implemented by using HOE-based substrate guided wave optical interconnects. In Section 2, we discuss the mathematical background of the PS. An experiment is given in Section 3 to demonstrate the PS interconnection using HOE-based substrate guided wave optical interconnects. A multistage shuffle network combining such a planarized PS architecture and smart pixel switching arrays is proposed in Section 4. A conclusion is given in Section 5.

2. The Perfect Shuffle Interconnection

For a computing cluster having $N = 2^k$ processing elements, the PS-bared optical interconnection divides this group into two subgroups and then interlaces the PEs from the first subgroup to the second subgroup with a one-to-one interconnection. The PS is generally defined mathematically as[1]

$$n' = \begin{cases} 2n & \text{for } 0 \le n \le N/2-1; \\ 2n-N+1 & \text{for } N/2 \le n \le N-1, \end{cases} \qquad (1)$$

where n' is the new location of the nth PE. An interconnection of a PS having 8 PEs is shown in Figure 1. The first PE subgroup located at 0, 1, 2, 3 will be shuffled to new positions numbered by 0, 2, 4, 6, respectively. The other subgroup with locations 4, 5, 6, 7 will be interlaced to positions 1, 3, 5, 7, respectively. Assume the distance between the two adjacent PEs in both input and output nodes is a and the distance separating the input and output nodes is b, as shown in Figure 1, the angle α_n steering an input signal to its designated output nodes is given by

$$\alpha_n = \begin{cases} \tan^{-1}\left(\frac{na}{b}\right) & \text{for } 0 \le n \le N/2-1; \\ \tan^{-1}\left[\frac{(n-N+1)a}{b}\right] & \text{for } N/2 \le n \le N-1. \end{cases} \qquad (2)$$

Equ. (2) is used in our experiment for fabricating the corresponding HOEs.

3. Experiment

DuPont photopolymers HRF 600X001-20 (20 μm thick) are selected as the holographic films due to their dry processing, long shelf life, good photospeed, and large index modulation properties[11-14]. This type of material is advantageous when considering the wet-processing requirement affiliated with DCG[15]. The volume holographic grating formation mechanism in the photopolymer is known to be a three-step process.[11] First, an initial exposure records the interference pattern, which causes initial polymerization and diffusion of the monomer molecules to the bright fringe area from the dark fringe neighborhood within the photopolymer. A higher concentration of polymerization means a higher refractive index. Second, a uniform UV light is required for dye bleaching and complete polymerization of the photo-sensitive polymer. Third, a baking process further enhances the index modulation of the hologram formed.

To experimentally carry out the PS with eight pairs of PEs shown in Figure 1 using HOE-based substrate guided wave optical interconnects, eight input HOEs are integrated on a glass substrate to direct the input signals to the desired directions. The signals are eventually coupled out of the substrate by another corresponding output HOEs as shown in Figure 2. A two-beam interference method[10] is employed to fabricate both the input and output HOEs. An Argon ion laser operating at 514 nm is used in the hologram recording. For demonstration purpose, the reconstruction wavelength is set at 632.8 nm. The diffraction angle for each HOE, which is greater than the critical angle of a BK7 glass wave guiding plate, is designed to be

$$\theta_n = \tan^{-1}\left(\frac{L_{n'n}}{2md}\right), \qquad (3)$$

where $L_{n'n}$ is the distance interconnecting n'th and nth HOEs, d is the thickness of the substrate glass, and m is an integer representing the maximum number of the zig-zag bouncing with a distance of $2d\tan(\theta_n)$ in the substrate between the n'th and the nth HOEs. The Bragg condition[16] and the Snell's law are applied to calculate the diffraction angle in the holographic medium and then to convert the recording angles to those in the air. For each interconnection, two individual photopolymer films are laminated on the wave guiding plate (~3.35 mm thick) at the designated positions and volume holograms are then recorded in the films. An optical signal coupled in by an input HOE is totally internal-reflected and then correctly guided within the wave guiding plate at a diffraction angle defined by Eq. (3). The zig-zagged signal beam is finally coupled out by the output HOE. Eight pairs of HOEs are sequentially fabricated on the same wave guiding plate at the desired locations as indicated in Figure 2. The

integration of the HOEs on a solid wave guiding substrate makes the PS robust to mechanical and environmental perturbations when compared with free-space interconnects and which, with a surface normal configuration, makes the optoelectronic packaging much more reliable in conjunction with the surface-mount technology (SMT). In our experiment, the angles of rotation for eight pairs of HOEs are designed to be 0° ($0\rightarrow0$), 20.5° ($1\rightarrow2$), 37° ($2\rightarrow4$), 48.3° ($3\rightarrow6$), -48.3° ($4\rightarrow1$), -37° ($5\rightarrow3$), -20.5° ($6\rightarrow5$), and 0° ($7\rightarrow7$), the two numbers within the parenthesis are the corresponding input and output nodes, respectively; and the corresponding bouncing angles are 45° (n=0), 46.3° (n=1), 43°(n=2), 43.2° (n=3), 43.2° (n=4), 43° (n=5), 46.3° (n=6), and 45° (n=7).

Table 1 Interconnection allocations among input and output nodes

n	0	1	2	3	4	5	6	7
n'	0	2	4	6	1	3	5	7

Eight input beams with s-polarization are used as the input optical signals for the PS device. Table 1 gives the interconnection nodes between input and output optical signals. Figure 3(a) shows the transform of the first subgroup ($0\rightarrow0$, $1\rightarrow2$, $2\rightarrow4$, $3\rightarrow6$). Other permutations corresponding to the second subgroup ($4\rightarrow1$, $5\rightarrow3$, $6\rightarrow5$, $7\rightarrow7$) are shown in Figure3(b). In Figure 3, The input optical signals are also included in the photos to clearly show the PS operation. The diffraction efficiencies of all HOEs are measured and the results are shown in Figure 4. All data are within 80% $\pm$ 5%. The surface-normal input signals are diffracted by the input HOEs and are successfully coupled out in the surface-normal direction at the desired locations. Among all the interconnect scenarios, there is no crosstalk observed.

4. Discussion and Future Work

The planarized architecture with surface normal configuration is pivotal for implementing surface normal transceivers such as vertical cavity surface emitting lasers (VCSELs)[17, 18] and resonant cavity photodetectors[19]. Other than the PS interconnection for parallel processing algorithms, this method can also be used to implement other communication networks critical to parallel computing. There include butterfly and crossover interconnections, and multistage networks[20-23].

Figure 5 proposes an example of multistage shuffle network implemented with the planarized optical PS and the VCSEL based smart pixel arrays. The surface-normal configuration of the planarized PS make the surface mount technology readily available to integrate the surface-normal smart pixel arrays on the planar waveguiding substrate. Three stages are used to fulfill the routing function among the eight input channels (for a network system containing two-input and two-output switching nodes, a total of $\log_2(N)$ stages are needed to connect N input channels). The identical interconnection scheme for each PS link stage makes this optical network highly manufacturable and modularable. In each stage, four 2x2 active switches are employed to achieve the functionality of detecting, bypass/exchange switching, and reemitting optical signals. These active switching nodes are the VCSEL based smart pixel arrays monolithically integrated MSM photodetectors, transistors, and VCSELs. The performance of the smart pixel arrays is critical to this kind of shuffle network. In 1995, a photonic switch integrating a VCSEL, MSM photodetector and MESFET circuits is developed[24]. It was fabricated monolithically on a semi-insulating 2-inch GaAs substrate, in which the VCSEL is 15 μm in diameter, and the MSM photodetector is 20 μm square. The three MESFETs performs the thresholding and amplifier functions. The gate length of the MESFETs is 1 μm. The smart pixel can perform both NOR- and OR-type operations with a high contrast ratio of more than 30 dB with optical gain. A 3-dB bandwidth of 220 MHz at a 300 mW input light and switching energy of 700 fJ at a 100 MHz frequency is demonstrated. The abrupt thresholding characteristics, optical gain and small wavelength sensitivity are good for digital operations when there are cascaded connections between devices. Most recently, ~1 Gb/s data rate is reported for an integration of VCSELs with heterojunction bipolar transistors (HBT) and resonant photodetectors[25]. It is expected that higher switching speed (multi-GHz) smart pixel arrays will be developed in few years for practical usage.

5. Conclusion

An approach to implement the optical PS interconnection by the photopolymer HOE based substrate guided wave optical interconnects is proposed. Preliminary experimental results operating at 632.8 nm proves the feasibility. Several advantages are demonstrated using this method. First, the perfect shuffle interconnection can be easily achieved by the surface-normal input and output HOEs integrated on the wave guiding plate. The photopolymer films employed can be easily laminated on the substrate. Second, the integration of the HOEs on a solid wave guiding substrate makes the PS robust against mechanical and environmental perturbations when compared with free-space interconnects and which makes the optoelectronic packaging much more reliable. Finally, the surface-normal configuration makes easy the integration with VCSEL based smart pixel arrays, and other surface-mountable processing elements to achieve multistage networks.

Acknowledgments

This work is supported by AFOSR, BMDO, ONR, Cray Research, DuPont, and the ATP program of the state of Texas.

References

1. H. S. Stone, "Parallel processing with the perfect shuffle," IEEE Trans. Comput. **C-20**, 153-161 (1971).
2. J. W. Goodman, F. I. Leonberger, S. Y. Kung, and R. A. Athale, "Optical interconnection for VLSI systems," Proc. IEEE **72**, 850-866 (1984).
3. T. Yatagai, S. Kawai, and H. Huang, "Optical computing and interconnects," Proc. IEEE **84**, 828-852 (1996).
4. A. W. Lohmann, "What classical optics can do for the digital optical computer," Appl. Opt. **25**, 1543-1549 (1986).
5. A. W. Lohmann, W. Stork, and G. Stucke, "Optical perfect shuffle," Appl. Opt. **25**, 1530-1531 (1986).
6. A. A. Sauchuk and J. Glaser, "Geometries for optical implementations of the perfect shuffle," Proc. SPIE, **963**, 270-282 (1989).
7. H. Kang, Y. Zhan, J. Zhang, X. Huang, and X. Zhu, "Optical perfect-shuffle network implementation by use of an ordinary imaging system and holographic gratings," Appl. Opt. **33**, 2988-2990 (1994).
8. N. Davidson, A. A. Friesem, and E. Hasman, "Realization of perfect shuffle and inverse perfect shuffle transforms with holographic elements," Appl. Opt. **31**, 1810-1812 (1992).
9. J. M. Wang, L. Cheng, and A. A. Sawchuk, "Light-efficient two-dimensional perfect shuffles with DuPont photopolymer holograms," Appl. Opt. **32**, 7148-7154 (1993).
10. Ray T. Chen, C. Zhou, C. Zhao, and R. Lee, "Photopolymer-based waveguide holograms for optoelectronic interconnects applications," Critical Reviews of Optical Science & Technology **CR 63**, 46-64 (1996).
11. W. Gambogi, K. Steijn, S. Mackara, T. Duzik, B. Hamzavy, and J. Kelly, "HOE imaging in DuPont holographic photopolymers," Proc. SPIE 2152, 282-293 (1994).
12. U. Rhee, H. J. Caulfield, C. S. Vikram, and J. Shamir, "Dynamics of hologram recording in DuPont photopolymer," Appl. Opt. **34**, 846-853 (1995).
13. S. Piazzolla and B. K. Jenkins, "Holographic grating formation in photopolymers," Opt. Lett. **21**, 1075-1077 (1996).

14. H. J. Zhou, V. Morozov, and J. Neff, "Characterization of DuPont photopolymers in infrared light for free-space optical interconnects," Appl. Opt. **34**, 7457-7459 (1995).
15. T. G. Georgekutty and H. K. Liu, "Simplified dichromated gelatin hologram recording process," Appl. Opt. **26**, 372-376 (1987).
16. H. Kogelnik, "Coupled wave theory for thick hologram gratings," The Bell Sys. Tech. J. **13**. 2909-2947 (1969).
17. D. L. Huffaker, L. A. Graham, and D. G. Deppe, "Fabrication of high-packing-density vertical cavity surface emitting laser arrays using selective oxidation," IEEE Photon. Technol. Lett. **8**, 596-598 (1996).
18. D. G. Deppe, D. L. Huffaker, J. Shin, and Q. Deng, "Very-low-threshold index-confined planar microcavity lasers," IEEE Photon. Technol. Lett. **7**, 965-967 (1995).
19. Hui Nie, K. A. Anselm, C. Hu, S. S. Murtaza, B. G. Streetman, and J. C. Campbell, "High-speed resonant-cavity seperate absorption and multiplication avalanche photodiodes with 130 GHz gain-bandwidth product," Appl. Phys. Lett. **70**, 161-163 (1997).
20. C. Tocci and H. J. Caulfield, *Optical Interconnection*. Artech House (Boston), 1994.
21. D. G. Sun, N. Wang, L. He, M. Xu, G. Liang, and J. Zheng, "Research on optical multistage butterfly interconnection and optoelectronic logic operations," Opt. Laser Technol. **26**, 379-383 (1994).
22. T. J. Cloonan, G. W. Richards, R. L. Morrison, A. L. Lentine, J. M. Sasian, F. B. McCormick, S. J. Hinterlong, and H. S. Hinton, "Shuffle-equivalent interconnection topologies based on computer-generated binary-phase gratings," Appl. Opt. **33**, 1405-1430 (1994).
23. F. B. McCormick, T. J. Cloonan, A. L. Lentine, J. M. Sasian, R. L. Morrison, M. G. Beckman, S. L. Walker, M. J. Wojcik, S. J. Hinterlong, R. J. Crisci, R. A. Novotny, and H. S. Hinton, "Five-stage free-space optical switching network with field-effect transistor felf-electro-optic-effect-device smart-pixel arrays," Appl. Opt. **33**, 1601-1618 (1994).
24. S. Matsuo, T. Nakahara, Y. Kohama, Y. Ohiso, S. Fukushima, and T. Kurokawa, "Monolithically integrated photonic switching device using an MSM PD, MESFET's, and a VCSEL," IEEE Photon. Technol. Lett. **7**, 1105-1107 (1995).
25. J. Cheng, Y. C. Lu, B. Lu, G. G. Ortiz, A. C. Alduino, and C. P. Hains, "High-speed transceiver and routing switch using VCSEL-based integrated optoelectronics," SPIE **3005**, 327-333 (1997).

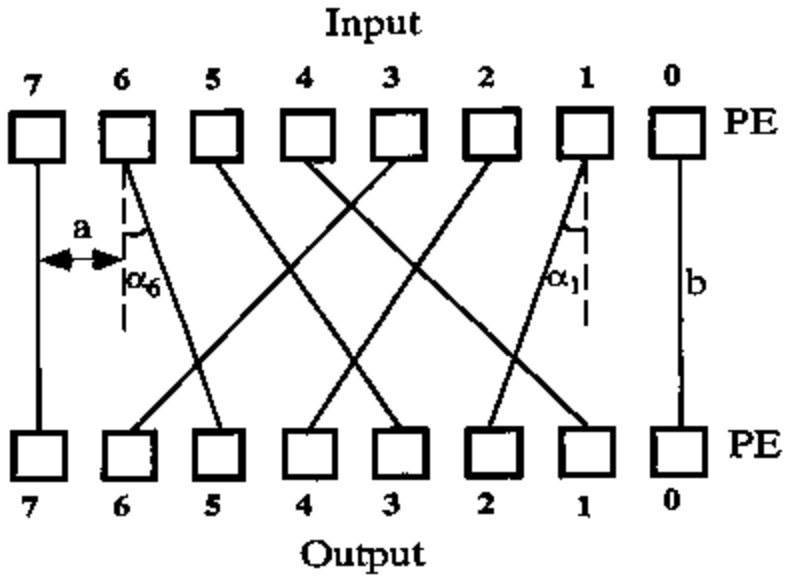

Figure 1 Schematic diagram for the perfect shuffle (PS) interconnection with N = 8 processing elements (PEs). The small boxes represent PEs.

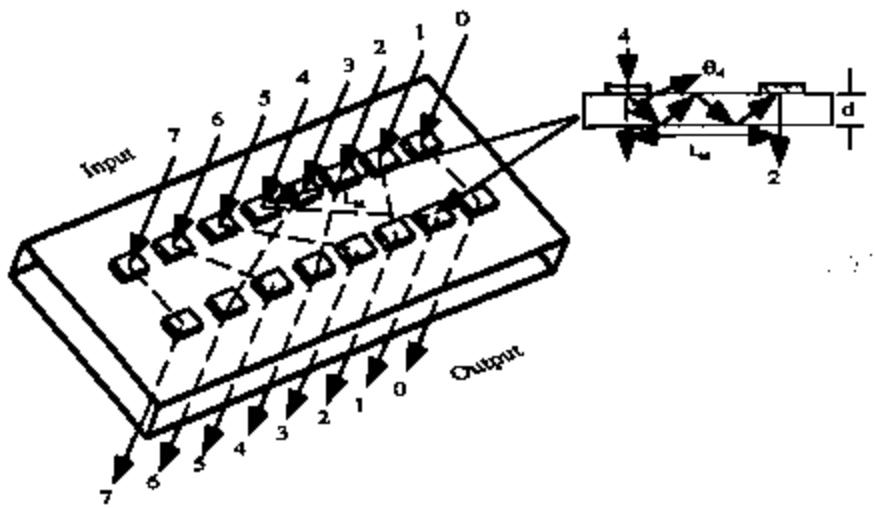

Figure 2 Integration of 8 pairs of holographic optical elements (HOEs) on one waveguiding plate. Interconnection in the waveguiding plate between the 4th PE of the input group and 1st PE of the output group is shown in the inset as an example.

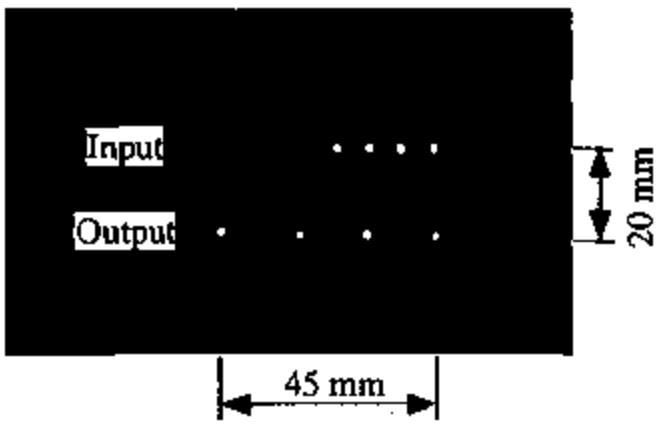

(a)

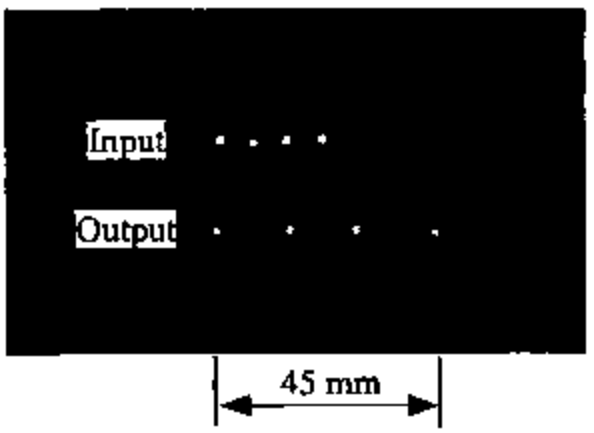

(b)

Figure 3 Experimental results of the PS interconnection with 8 PEs.
(a) interconnecting result for the first subgroup;
(b) interconnecting result for the second subgroup.

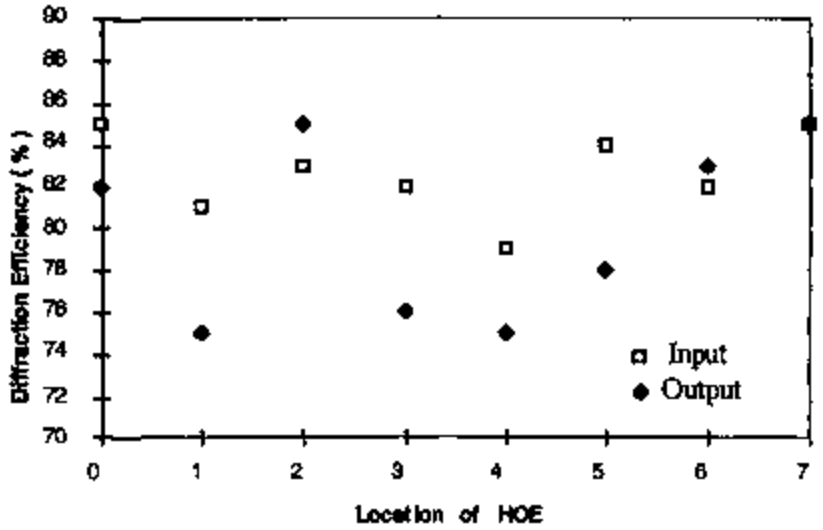

Figure 4 Measured diffraction efficiencies for the 8 pairs of HOEs

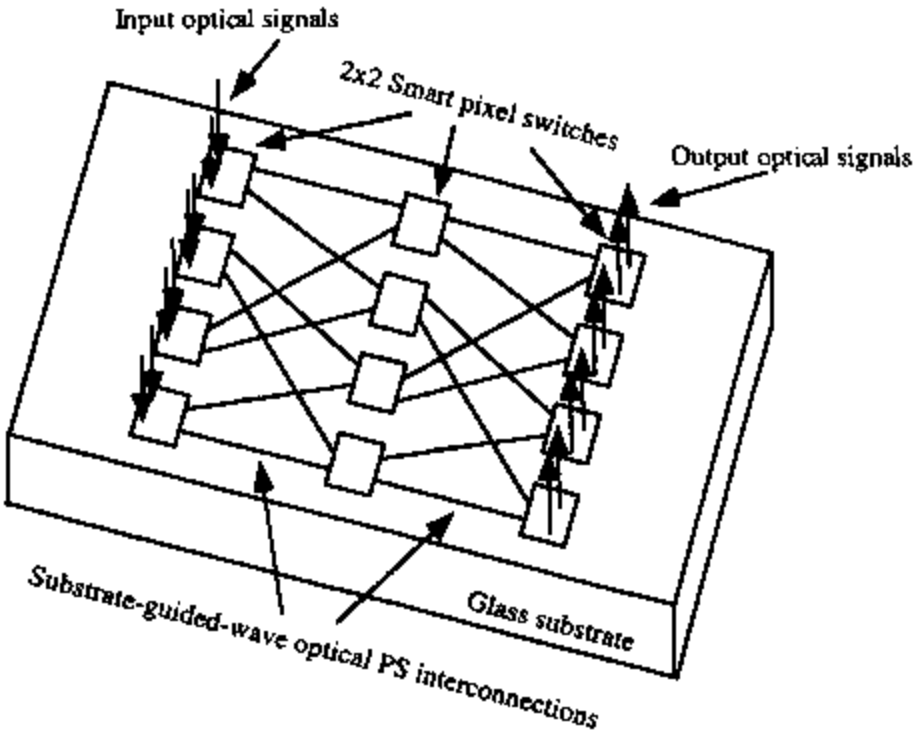

Figure 5 Schematic diagram for a three stages shuffle network